# Function of UreB in *Klebsiella aerogenes* Urease

Eric L. Carter,[†] Jodi L. Boer,[‡] Mark A. Farrugia,[‡] Nicholas Flugga,[†] Christopher L. Towns,[†] and Robert P. Hausinger*,[†,‡]

[†]Department of Microbiology and Molecular Genetics and [‡]Department of Biochemistry and Molecular Biology, Michigan State University, East Lansing, Michigan 48824, United States

ABSTRACT: Urease from *Klebsiella aerogenes* is composed of three subunits (UreA−UreB−UreC) that assemble into a $(UreABC)_3$ quaternary structure. UreC harbors the dinuclear nickel active site, whereas the functions of UreA and UreB remain unknown. UreD and UreF accessory proteins previously were suggested to reposition UreB and increase the level of exposure of the nascent urease active site, thus facilitating metallocenter assembly. In this study, cells were engineered to separately produce $(UreAC)_3$ or UreB, and the purified proteins were characterized. Monomeric UreB spontaneously binds to the trimeric heterodimer of UreA and UreC to form $(UreABC^*)_3$ apoprotein, as shown by gel filtration chromatography, integration of electrophoretic gel band intensities, and mass spectrometry. Similar to the authentic urease apoprotein, the active enzyme is produced by incubation of $(UreABC^*)_3$ with Ni^{2+} and bicarbonate. Conversely, UreBΔ1−19, lacking the 19-residue potential hinge and tether to UreC, does not form a complex with $(UreAC)_3$ and yields negligible levels of the active enzyme when incubated under activation conditions with $(UreAC)_3$. Comparison of activities and nickel contents for $(UreAC)_3$, $(UreABC^*)_3$, and $(UreABC)_3$ samples treated with Ni^{2+} and bicarbonate and then desalted indicates that UreB facilitates efficient incorporation of the metal into the active site and protects the bound metal from chelation. Amylose resin pull-down studies reveal that MBP-UreD (a fusion of maltose binding protein with UreD) forms complexes with $(UreABC)_3$, $(UreAC)_3$, and UreB in vivo, but not in vitro. By contrast, MBP-UreD does not form an in vivo complex with UreBΔ1−19. The soluble MBP-UreD−UreF−UreG complex binds in vitro to $(UreABC)_3$, but not to $(UreAC)_3$ or UreB. Together, these data demonstrate that UreB facilitates the interaction of urease with accessory proteins during metallocenter assembly, with the N-terminal hinge and tether region being specifically required for this process. In addition to its role in urease activation, UreB enhances the stability of UreC against proteolytic cleavage.
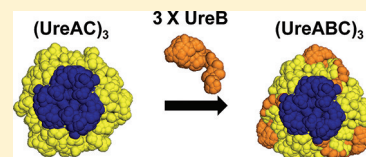
Urease hydrolyzes urea to ammonia and carbamic acid, with the latter compound spontaneously decomposing to form a second molecule of ammonia and carbonic acid.[1,2] Of medical importance, the human gastric ulcer-causing bacterium *Helicobacter pylori* employs urease as an essential virulence factor during colonization of stomach tissue, and uropathogens commonly produce urease that is directly related to stone formation and pyelonephritis.[3] This enzyme is also important in agriculture as seed germination is accompanied by release of urea that must be decomposed via plant urease for subsequent nitrogen assimilation, and urease produced by soil-borne microbes catalyzes the spurious degradation of urea-containing fertilizers.[4,5] Furthermore, urease has historical and basic research significance: it was the first enzyme to be crystallized[6] and the first shown to contain nickel,[7] a cofactor essential for its activity.

The in vivo maturation of urease requires the concerted effort of several accessory proteins, a process that has served as a paradigm for metallocenter assembly.[1,2] In the best-studied model system, that involving the expression of *Klebsiella aerogenes* urease genes (*ureDABCEFG*) in *Escherichia coli*, the metallochaperone UreE[8] delivers Ni^{2+} to an activation complex consisting of the $(UreABC)_3$ urease apoprotein along with UreD, a molecular chaperone that is thought to alter the urease apoprotein conformation and also binds metal,[9,10] UreF, a putative GTPase activating protein,[11−13] and UreG, a Ni^{2+}- and Zn^{2+}-binding GTPase.[14,15] In a process that is not well understood, CO_2 forms a Lys−carbamate bridging ligand at the nascent active site, GTP is hydrolyzed by UreG, Ni^{2+} is transferred from UreE (possibly via UreG and UreD) to the appropriate ligands in $(UreABC)_3$, and the accessory proteins dissociate, providing the fully active holoprotein. Additional studies hint that a UreD−UreF−UreG heterotrimeric complex interacts with the urease apoprotein, rather than the sequential binding of the individual accessory proteins.[1,10,15]

Various forms of the urease apoprotein are partially activated in vitro by incubation with excess bicarbonate (as a CO_2 donor) and Ni^{2+} ions. Whereas $(UreABC)_3$ is activated under optimized conditions to levels representing ∼16% of that of the fully active enzyme (i.e., ∼400 units/mg of protein vs 2500 units/mg of protein, where units are micromoles of urea degraded per minute at 37 °C), the $(UreABC)_3$−UreD, $(UreABC)_3$−UreD−UreF, and $(UreABC)_3$−UreD−UreF−UreG complexes are activated to ∼25, ∼30, and ∼50%, respectively, of this level.[16−19] Furthermore, incubation of the $(UreABC)_3$−UreD−UreF−UreG complex with UreE, Mg^{2+}-GTP, and physiologically relevant levels of Ni^{2+} and bicarbonate leads to wild-type levels of activity.[20] These results illustrate the importance of accessory proteins, Mg^{2+}-GTP, and CO_2 in the efficient assembly of the urease active site.

Crystal structures of urease from *K. aerogenes*,[21,22] *Bacillus pasteurii*,[23,24] *H. pylori*,[25] and jack bean (*Canavalia ensiformis*)[26] have been determined, each revealing highly similar tertiary structures and essentially identical active sites containing a dinuclear nickel metallocenter bridged by a Lys−carbamate and a solvent molecule (the *K. aerogenes* structure is shown in Figure 1). A related urease from *Helicobacter mustelae* has been structurally characterized and shown to contain a dinuclear iron metallocenter.[27] In *K. aerogenes* urease, the 60.3 kDa UreC subunit harbors the active site while the UreA and UreB small subunits (11.1 and 11.7 kDa, respectively) have no obvious role in catalysis but contribute to the overall (UreABC)₃ quaternary structure. The function of each subunit (or protein domain for ureases in which the subunits are fused) is likely the same for ureases from different organisms.

Studies focused on the interaction of accessory proteins with *K. aerogenes* urease have provided potential insights into a role for UreB during urease activation. In a chemical cross-linking investigation, amine group-specific reagents were used to treat several urease apoprotein complexes, followed by mass spectrometric analysis of tryptic peptides.[28] In particular, a cross-link was detected in the (UreABC)₃−UreD−UreF complex between UreB Lys76 and UreC Lys382, residues that are distant from each other in the enzyme crystal structure. This finding was interpreted as indicating a UreD−UreF-induced conformational change in UreB, where the shift in its position allows greater access to the buried active site by CO_2 and Ni^{2+} (e.g., note the increased accessibility of the nickel atoms after removal of UreB from the crystal structure in Figure 1D). The UreB-shift hypothesis was supported by ProFlex computational analysis that identified increased flexibility of UreB residues 11−19.[29] This region was predicted to be a hinge that potentially allowed UreB's main domain, which exhibited only weak interactions with UreC, to move while remaining anchored via residues 2−8. Additional structural evidence of UreB's role is derived from small-angle X-ray scattering of (UreABC)₃−UreD and (UreABC)₃−UreD−UreF complexes; modeling of the data indicates UreD and UreF are positioned near UreB at the vertices of the triangular apoprotein.[29] Together, these results point to UreB playing a crucial role during the in vivo activation of the urease apoprotein.

In this study, *K. aerogenes* UreB and the complex of UreA with UreC [(UreAC)₃] were purified individually and shown to be capable of forming a stoichiometric complex in vitro. The resulting (UreABC*)₃ apoprotein shares similar in vitro activation properties with the authentic apoprotein purified from the cell. Additionally, metal analyses and activity assays of various activated species demonstrate that UreB is required for the efficient incorporation of Ni^{2+} into the active site and stabilizes the site against metal chelation. We also examine the protein−protein interaction network of UreB with other urease components in vivo and in vitro and show that UreB is partially responsible for the interaction of (UreABC)₃ with accessory proteins. Furthermore, we show that a UreB truncation mutant lacking the proposed hinge and tether region (i.e., N-terminal residues 1−19) is unable to associate with (UreAC)₃ or a soluble form of UreD. These results highlight the importance of UreB, especially its N-terminus, for forming an interface with urease accessory proteins. Together, these data implicate UreB as a key player in facilitating the interaction of accessory proteins with urease apoprotein and directing the efficient incorporation of Ni^{2+} into the nascent active site. In addition, we show that UreB stabilizes urease against proteolytic cleavage.
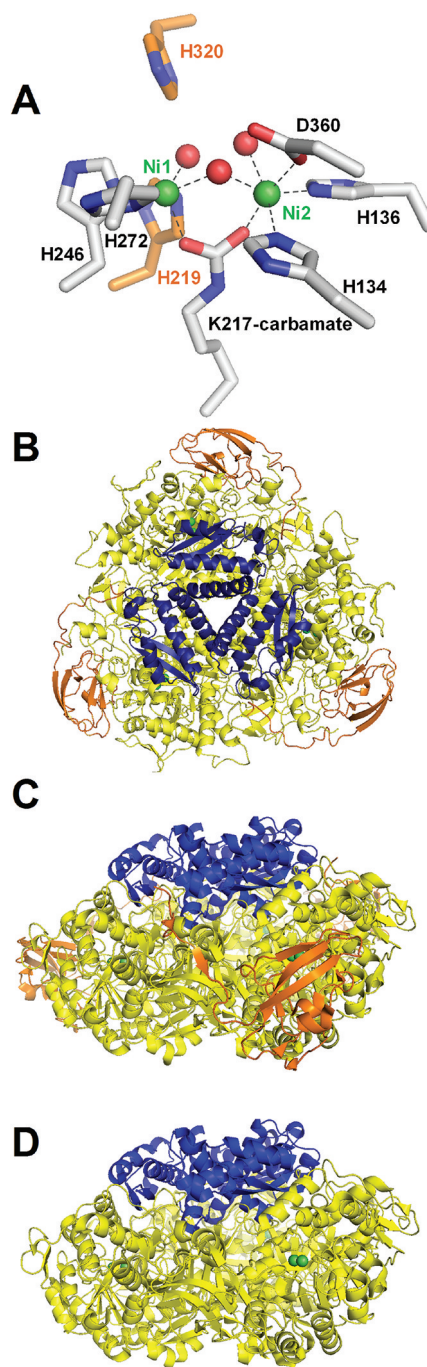
Figure 1. Structure of *K. aerogenes* urease. (A) Dinuclear nickel active site of urease. The two nickel atoms (green) are bridged by a Lys-carbamate and a hydroxyl group. Ni1 also is coordinated by two His residues and a terminal solvent, while Ni2 also has two His residues, an Asp, and a terminal water. Waters are colored red; metal-binding side chains are depicted with white carbons, and two nearby His residues that function in catalysis are shown with orange carbons. (B and C) Two views of the (UreABC)₃ cartoon structure with UreA colored blue, UreB orange, UreC yellow, and nickel atoms green. (D) Same view as panel C, but with the UreB subunits removed. Figures were prepared using PYMOL and Protein Data Bank entry 1FWJ.

■ EXPERIMENTAL PROCEDURES

Plasmid Construction. Standard molecular biology techniques were employed for construction of the plasmids described below and are summarized in Table 1.[30] Polymerase

Table 1. Characteristics of Plasmids Used in These Studies

name	relevant characteristics	ref
pKK17	*K. aerogenes* ureDABCEFG cloned into pKK223-3	31
pET-42b	T7 RNA polymerase-driven expression vector with a pBR322 origin of replication	Merck
pUreB	pET-42b containing full-length *ureB*	this work
pUreBΔ1–19	pET-42b containing 5′-truncated *ureB* that encodes Met and UreB residues 20–106	this work
pETDuet-1	expression vector with two multiple cloning sites with independent T7 RNA polymerase-driven transcription units for the simultaneous production of two proteins in the cell	Merck
pUreAC	pETDuet-1 with *ureA* and *ureC* inserted into the two multiple-cloning sites	this work
pCDF-1b	T7 RNA polymerase-driven expression vector with a CloDF13 origin of replication	Merck
pCDF-MBP-UreD	*malE-ureD* cloned into pCDF-1b to produce MBP-UreD with an N-terminal His$_6$ tag	this work
pKAU22ΔureD-1	*K. aerogenes* ureDABCEFG cloned into pUC18	43
pEC002	pMal-c2x with *ureD* cloned after, and in transcriptional fusion with, *malE* to encode MBP-UreD	10
pEC004	*ureABC* cloned into pACT3	10
pEC005	*ureFG* cloned into pACT3	10

chain reaction (PCR) was conducted with oligonucleotide primers purchased from IDT DNA (Coralville, IA) and *Pfu*Turbo Hotstart PCR Master Mix (Stratagene). *E. coli* DH5α (Invitrogen) was the host bacterial strain for cloning manipulations, and plasmids were verified by sequence analysis (Davis Sequencing, Davis, CA).

For the overproduction of UreB, pUreB was constructed by PCR amplification using a forward primer (5′-GGAGATA-TACCAC*ATATG*ATCC-3′) containing an NdeI restriction site (in italics), a reverse primer (5′-TGATGC*AAGCTT*CTAT-TACTCATCG-3′) containing a HindIII restriction site, and pKK17 as a template.[31] The resultant amplicon encoding full-length *ureB* (followed by successive ochre and amber stop codons for increased transcriptional termination efficiency) was digested with NdeI and HindIII, with the resultant *ureB*-containing fragment ligated into similarly digested pET-42b (Merck, Darmstadt, Germany).

To assess the function of the putative hinge and tether region of UreB encompassing N-terminal residues 1–19, pUreBΔ1–19 was constructed by PCR amplification using a forward primer (5′-AGCTACGAGC*ATATG*GCAACCTGTCGCGTG-GTCGTTGAGAACCACGGCGATC-3′) containing an NdeI restriction site, a reverse primer (5′-TATA*GGATCC*CTATTAC-TCATCGTTTACCTCCAGAGGGCCCATGACC-3′) containing a BamHI restriction site (with tandem ochre and amber stop codons), and pUreB as a template. The resultant amplicon was digested with NdeI and BamHI, and the desired fragment was ligated into similarly digested pET-42b. pUreBΔ1–19 encodes a Met residue followed by UreB residues 20–106.

To produce urease lacking UreB, the pUreAC vector was constructed coding for *ureA* and *ureC*. The *ureA* gene was amplified by using a forward primer (5′-AGTCAGAGC*CATG*G-AACTGACCCCCCGAC-3′) containing an NcoI restriction site, a reverse primer (5′-AGTCAGAGC*TTAAG*TCAGATAA-TCGGGTTGTGAACG-3′) containing an AflII restriction site, and pKK17 as a template. Similarly, *ureC* was amplified by using a forward primer (5′-AGCTACGAGC*ATATG*AGTAAT-ATTTCACGC-3′) containing an NdeI restriction site, a reverse primer (5′-AGTCAGAG*TTAATTAA*AACAGAAAATAT-CGTTG-3′) containing a PacI restriction site, and pKK17 as template. The resulting amplicons were digested with their respective restriction endonucleases, and the appropriate fragments were stepwise ligated into similarly digested pETDuet-1 (Merck).

For studies focusing on the interaction of UreD with (UreAC)$_3$, UreB, and UreBΔ1–19, pCDF-MBP-UreD was constructed

by amplifying the *malE-ureD* transcriptional fusion from pEC002,[10] using a forward primer (5′-GCATA*GGTACC*ATG-AAAATCG-3′) containing a KpnI restriction site and a reverse primer (5′-TATA*AAGCTT*TTAAGTCAGCCAGATTCGGG-GAAG-3′) containing a HindIII restriction site. The resultant amplicon was digested with KpnI and HindIII, and the desired fragment was ligated into similarly digested pCDF-1b (Merck). pCDF-MBP-UreD encodes full-length MBP-UreD with an N-terminal His$_6$ tag.

Urease Activity and Protein Assays. Urease activity was determined by measuring the rate of ammonia production, monitored by its conversion to indophenol with quantification at 625 nm.[32] Aliquots of a reaction mixture consisting of 50 mM 4-(2-hydroxyethyl)piperazine-1-ethanesulfonic acid (HEPES) (pH 7.8), 50 mM urea, 0.5 mM ethylenediaminete-traacetic acid (EDTA), and protein were removed at selected times and mixed with an alkaline solution of phenol and sodium nitroprusside. Protein concentrations were determined by using the Protein Assay reagent (Bio-Rad) with bovine serum albumin as a standard.

Polyacrylamide Gel Electrophoresis and Western Blot Analysis. Sodium dodecyl sulfate–polyacrylamide gel electro-phoresis (SDS–PAGE) was performed by using standard buffers[33] and 12% polyacrylamide running gels with 4% stacking gels. Proteins were visualized with Coomassie brilliant blue stain. For Western blot analysis, SDS–PAGE gels were electroblotted onto Immobilon-P polyvinylidene difluoride membranes (Millipore) and blotted with anti-*K. aerogenes* urease antibodies.[34] Reactive protein bands were visualized with anti-rabbit IgG alkaline phosphatase-conjugated antibodies and 5-bromo-4-chloro-3-indolyl phosphate/nitroblue tetrazolium liquid substrate (Sigma). Whereas the antibodies react strongly with UreB and UreC, they react only weakly with UreA. Gel scanning was conducted by using AlphaEaseFC (Alpha Innotech Corp., San Leandro, CA) and assuming the following molecular masses: 11.1 kDa for UreA, 11.7 kDa for UreB, 9.8 kDa for UreBΔ1–19, and 60.3 kDa for UreC. Molecular mass markers for Coomassie-stained gels and Western blots were purchased from Bio-Rad.

Protein Purification. UreB was purified from *E. coli* BL21-Gold(DE3) cells (Stratagene) harboring pUreB and grown in Lennox Broth (LB; Fisher Scientific) supplemented with 50 μg/mL kanamycin with shaking at 37 °C until the cells reached an optical density at 600 nm (OD$_{600}$) of ∼0.5. Protein production was induced by the addition of 0.5 mM isopropyl β-D-1-thiogalactopyranoside (IPTG). The cultures were incubated

overnight and harvested by centrifugation. Cell pellets were suspended in PEB buffer [20 mM sodium phosphate (pH 7.4), 1 mM EDTA, and 1 mM 2-mercaptoethanol (β-ME)] and disrupted by sonication using a Branson sonifier (three or four cycles, 2 min per cycle, 50% duty cycle, power level 3-5, and cooling in an ice/water/ethanol bath between cycles). Soluble cell-free extracts were obtained by centrifugation of the cell lysate for 45−60 min at 120000g and applied to DEAE-Sepharose (2.5 cm × 13 cm; GE Healthcare) equilibrated in PEB. Unbound species were allowed to flow through before a linear gradient from 0 to 1 M KCl in PEB was run over ∼6 column volumes. UreB eluted in the latter portion of the flow-through fractions and the beginning of the linear gradient. Fractions containing UreB were verified by SDS−PAGE, pooled, and concentrated to ∼1 mL by using both an Amicon ultrafiltration stir cell equipped with a 10000 molecular weight cutoff (MWCO) membrane and a 10000 MWCO Amicon centrifugal filter device (Millipore). The sample was loaded onto a preparative Superdex-75 (GE Healthcare) column (1.5 cm × 68 cm) equilibrated in PEB. Fractions containing UreB were identified by SDS−PAGE, pooled, and buffer exchanged either by dialysis or by repeated concentration and dilution into HT buffer [50 mM HEPES (pH 7.8) and 1 mM tris(2-carboxyethyl)phosphine hydrochloride (TCEP)] before being snap-frozen in liquid N_2 prior to being stored at −80 °C. Protein stored in this manner was stable for at least 1 month.

UreBΔ1−19 was purified from *E. coli* BL21-Gold(DE3) harboring pUreBΔ1−19 by a process similar to that for UreB. In this case, however, the cells were supplemented with 1 mM IPTG and grown for an additional 3 h prior to being harvested by centrifugation.

UreAC [(UreAC)$_3$] was purified from *E. coli* BL21-Gold(DE3) harboring pUreAC and grown in LB supplemented with 300 μg/mL ampicillin with shaking at 37 °C until the cells reached an OD$_{600}$ of ∼0.5. Protein production was induced by the addition of 1 mM IPTG; the cultures were incubated under the same conditions for 3 h, and cells were harvested by centrifugation. Cell pellets were suspended in PEB buffer, and a soluble cell-free extract was prepared and chromatographed on DEAE-Sepharose as described above for the purification of UreB. (UreAC)$_3$ eluted at approximately the midpoint of the KCl gradient, similar to the anion-exchange chromatographic behavior of fully assembled urease, (UreABC)$_3$.[35] Fractions containing (UreAC)$_3$ were identified by SDS−PAGE, pooled, and adjusted to 1.5 M KCl by dialysis. The sample was filtered and applied to phenyl-Sepharose CL-4B (2.5 cm × 13 cm; GE Healthcare) equilibrated in PEB containing 1.5 M KCl. Unbound species were eliminated by washing with equilibration buffer before the bound (UreAC)$_3$ was eluted with PEB. Fractions containing (UreAC)$_3$ were identified by SDS−PAGE, pooled, buffer exchanged into HT, and stored like UreB. These samples also were stable for at least 1 month at −80 °C.

Urease apoprotein was purified from *E. coli* cells harboring pKAU22ΔureD-1 that were grown in LB supplemented with 300 μg/mL ampicillin with shaking at 37 °C overnight before being harvested by centrifugation. Cell pellets were suspended in PEB, and the remaining purification steps were performed as previously described,[10] except pure (UreABC)$_3$ was buffer exchanged into HT and stored like UreB and (UreAC)$_3$.

The soluble, heterotrimeric, MBP-UreD−UreF−UreG accessory protein complex was purified from *E. coli* BL21-Gold(DE3) cells harboring plasmids pEC002 and pEC005.[10] The former plasmid encodes MBP-UreD, and the latter encodes UreF and UreG. The cells were grown in LB supplemented with 300 μg/mL ampicillin and 50 μg/mL chloramphenicol with shaking at 37 °C until the OD$_{600}$ reached ∼0.4. Protein production was induced with 0.5 mM IPTG; the cultures were incubated at 28 °C with shaking for 16 h, and cells were harvested by centrifugation. Cell pellets were resuspended in TEB [20 mM 2-amino-2-(hydroxymethyl)-1,3-propanediol (Tris)-HCl (pH 7.5), 1 mM EDTA, and 1 mM β-ME] containing 25 mM NaCl and disrupted by sonication as described above. Soluble cell-free extracts were obtained by ultracentrifugation (under conditions identical to those for the purification of UreB) and loaded directly onto a 2.5 cm × 6.1 cm amylose resin column (New England Biolabs) equilibrated in resuspension buffer. The column was washed in the same buffer until the A_{280} reached baseline, and protein was eluted with 2 bed volumes of TEB containing 25 mM NaCl and 10 mM maltose. The eluted fractions of interest were pooled and loaded directly onto a DEAE-Sepharose column (2.5 cm × 13 cm) equilibrated in TEB. The column was washed with 1.5 bed volumes of TEB buffer before a linear gradient from 0 to 1 M NaCl was applied in the same buffer over ∼6 column volumes. Fractions containing the MBP-UreD−UreF−UreG complex were identified by SDS−PAGE, pooled, and concentrated by using a 10000 MWCO Amicon centrifugal filter device to a final volume of 1 mL. The sample was buffer exchanged into TEB containing 25 mM NaCl by dialysis and loaded onto a Superdex-200 column (1.5 cm × 68 cm) equilibrated in the same buffer. Elution fractions were analyzed by SDS−PAGE, and those containing the pure MBP-UreD−UreF−UreG complex were pooled and concentrated in the same manner as noted above.

MBP-UreD was purified from *E. coli* BL21-Gold(DE3) cells containing pEC002, as previously described.[10]

Complex Formation, Analytical Gel Filtration, and Matrix-Assisted Laser Desorption Ionization Time-of-Flight Mass Spectrometry (MALDI-TOF MS). Formation of a complex between (UreAC)$_3$ and either UreB or UreBΔ1−19 was monitored by gel filtration chromatography. In a 1 mL final volume of HT buffer, (UreAC)$_3$ (42 μM) was mixed with UreB or UreBΔ1−19 (208 μM). The mixture was incubated at room temperature for 15 min and chromatographed on a Superdex-200 column (1.5 cm × 68 cm) that was equilibrated in TBS [50 mM Tris-HCl (pH 7.4) and 150 mM NaCl] using a BioLogic LP System (Bio-Rad, Hercules, CA). The column eluant was monitored at 280 nm; fractions correlating to absorbance peaks were pooled and concentrated by using a 10000 MWCO Amicon centrifugal filter device, and the fractions were analyzed by SDS−PAGE.

The native molecular masses of (UreAC)$_3$ and UreB were estimated by using gel filtration chromatography. Samples (40 μL) of (UreAC)$_3$ (10 mg/mL) and UreB (1.2 mg/mL) in 50 mM sodium phosphate (pH 7.0) were chromatographed on a Shodex KW-804 column (8 mm × 300 mm; Shodex) equilibrated in the same buffer by using a Waters Breeze chromatography system while monitoring the A_{280} of the elution buffer. Another approach included chromatography of (UreAC)$_3$ (200 μL, 12.9 mg/mL) on a Superdex-200 column (1.5 cm × 68 cm) equilibrated in 20 mM Tris-HCl (pH 7.4), 1 mM EDTA, 1 mM β-ME, and 25 mM NaCl using a BioLogic LP System while monitoring the A_{280} of the elution buffer. Columns were standardized with a set of molecular mass markers (Bio-Rad). The retention times of the standards were plotted versus the logarithm of their molecular masses; the slope derived from the linear regression of the data points was

used to estimate the molecular mass of $(UreAC)_3$ or UreB based on the retention time of each.

To verify the protein content of gel filtration chromatography fractions, we employed MALDI-TOF MS. Samples of authentic urease apoprotein $(UreABC)_3$, $UreB\Delta1-19$, and selected gel filtration chromatography pools were buffer exchanged into deionized water and diluted to a final concentration of 1 μg/μL in 40% acetonitrile containing 0.1% trifluoroacetic acid. Samples were diluted 1:1 with a solution of 20 mg/mL sinapic acid prepared in 40% acetonitrile and 0.1% trifluoroacetic acid, and 2 μL samples of each preparation were spotted onto a Kratos Analytical MALDI MS plate and analyzed in a Shimadzu Axima CFR Plus MALDI-TOF mass spectrometer. Spectra were standardized with human insulin (MH^+ = 5808.7 Da) and apomyoglobin (MH^+ = 16952.6 Da).

Circular Dichroism (CD). $(UreAC)_3$ (10 μM heterodimer), UreB (100 μM), the complex derived from these species denoted $(UreABC^*)_3$ (10 μM heterotrimer), and $UreB\Delta1-19$ (100 μM) in HT buffer were diluted to the indicated concentrations in 50 mM sodium phosphate (pH 7.0). Parallel solutions containing the same mixtures of protein-free HT buffer and 50 mM sodium phosphate (pH 7.0) were used for establishing baselines. Samples (300 μL) were placed in a Spectrosil 1 mm quartz cuvette (Starna Cells) equipped with a stopper, and three or four scans were taken from 260 to 200 nm with 0.5 nm intervals and 20 s reads per interval in a Chirascan CD spectrometer (Applied Photophysics Limited, Leatherhead, U.K.) at ambient temperature. The baselines were subtracted, and the scans were averaged using Chirascan Pro-Data Viewer.

In Vitro Activation. $(UreAC)_3$ (10 μM heterodimer), $(UreABC)_3$ (10 μM heterotrimer), and $(UreABC^*)_3$ (5 μM heterotrimer) were incubated for 1 h at 37 °C in standard activation buffer [100 mM HEPES (pH 8.3), 150 mM NaCl, 100 mM $NaHCO_3$, and 100 μM $NiCl_2$] unless otherwise indicated. We prepared the $(UreABC^*)_3$ sample by incubating $(UreAC)_3$ (100 μM) with UreB (500 μM) in a 250 μL total volume of HT buffer at room temperature for 30 min, chromatographing the sample on Superdex-200 as described above, and identifying appropriate fractions by SDS−PAGE. Aliquots of the reaction mixtures were assayed for urease activity as described above.

To assess the effect of UreB on activity following the in vitro activation process, 10 μM $(UreAC)_3$ was activated for 60 min at 37 °C under standard conditions in a total volume of 100 μL prior to addition of 10 μL of UreB (520 μM stock) with an additional incubation for 60 min at 37 °C before aliquots were assayed for urease activity. Specific activities were calculated by using the concentration of the UreABC heterotrimer (i.e., 0.756 mg/mL) after the addition of UreB.

In addition, the effect of $UreB\Delta1-19$ on the in vitro activation process was examined. $(UreAC)_3$ (100 μM) was mixed with $UreB\Delta1-19$ (500 μM) in a 20 μL total volume of HT and incubated for 30 min at ambient temperature. A portion (10 μL) of this mixture was transferred into 90 μL of standard activation buffer, incubated at 37 °C for 60 min, and assayed for urease activity. Specific activities were calculated by using the concentration of UreAC heterodimer and stoichiometric $UreB\Delta1-19$ (i.e., 0.812 mg/mL), excluding the excess $UreB\Delta1-19$.

Metal Analysis of in Vitro Activated Species. To assess the nickel content of activated $(UreABC^*)_3$, we mixed 120 μL of $(UreAC)_3$ (370 μM heterodimer in HT buffer) with 120 μL

of UreB (1450 μM in HT buffer) and incubated the mixture for 30 min at ambient temperature. The mixture was diluted to ~10 μM UreC protomer with 4.2 mL of standard activation buffer and incubated at 37 °C for 60 min. The sample was concentrated with a 10000 MWCO Amicon centrifugal filter device (prewashed with deionized water) to ~300 μL and either immediately chromatographed on a 1 cm × 43 cm Sephacryl S300 HR column (GE Healthcare) equilibrated in 100 mM HEPES (pH 8.3) or treated with 10 mM EDTA for 5 min at ambient temperature and chromatographed in the same buffer with 1 mM EDTA. Fractions of interest were verified for protein content with SDS−PAGE, allowed to equilibrate for at least 16 h at 4 °C, concentrated by use of 10000 MWCO Amicon centrifugal filter devices, and analyzed in parallel with protein-free buffer for metal content by inductively coupled plasma-atomic emission spectroscopy (ICP-AES) (Chemical Analysis Laboratory, University of Georgia, Athens, GA).

For studies focusing on the nickel content of $(UreAC)_3$ after activation, a similar methodology was employed as described above except that $(UreAC)_3$ (120 μL, 370 μM in HT buffer) was directly diluted to a final UreC protomer concentration of ~10 μM in activation buffer prior to concentration, with or without EDTA treatment, and gel filtration chromatography. Lastly, 4.3 mL of $(UreAC)_3$ (UreC protomer final concentration of ~10 μM) was subjected to standard activation conditions at 37 °C for 60 min, mixed with 120 μL of UreB (1450 μM in HT buffer), incubated at ambient temperature for 30 min, and analyzed for nickel content after concentration, with or without EDTA treatment, and gel filtration chromatography as described above.

In Vivo Amylose Pull-Down Studies. Competent *E. coli* BL21-Gold(DE3) cells were transformed with pCDF-MBP-UreD by following the manufacturer's instructions (Stratagene) and maintained on LB agar supplemented with spectinomycin at 66 μg/mL. The preceding strain was made competent by using $CaCl_2$ and cotransformed with either pEC004,[10] pUreAC, pUreB, or $pUreB\Delta1-19$ by using a standard heat-shock transformation protocol.[30] The resultant cotransformants were maintained on LB agar with spectinomycin at 66 μg/mL with 50 μg/mL chloramphenicol for the maintenance of pEC004, 100 μg/mL ampicillin for pUreAC, or 50 μg/mL kanamycin for pUreB. An overnight culture (5 mL) was used to inoculate 500 mL of LB that was supplemented with the same antibiotics as described for each strain (except that 300 μg/mL ampicillin was used in liquid medium, rather than 100 μg/mL). The cells were grown with shaking at 37 °C to an OD_{600} of ~0.5, at which point protein production was induced with 1 mM IPTG. The cultures were incubated under the same conditions for an additional 3 h and harvested by centrifugation. Cell pellets were washed once with TBS and suspended in 15 mL of TEB containing 25 mM NaCl. The slurries were disrupted by sonication using a Branson sonifier (see above). Soluble cell-free extracts were obtained by ultracentrifugation at 120000g for 1 h and loaded onto a 5 mL bed volume, 1.5 cm diameter, amylose resin column equilibrated in TEB containing 25 mM NaCl. The column was washed with the same buffer until the A_{280} reached the baseline, at which point bound proteins were eluted in TEB containing 25 mM NaCl and 10 mM maltose. Elution fractions were pooled, concentrated with a 10000 MWCO Amicon centrifugal filter device, and examined by SDS−PAGE analysis.

In Vitro Amylose Pull-Down Studies. The MBP-UreD−UreF−UreG complex, $(UreABC)_3$, $(UreAC)_3$, and UreB were

dialyzed into TEB containing 25 mM NaCl. In a final volume of 250 μL, the MBP-UreD−UreF−UreG complex (2 μM) was mixed with (UreAC)$_3$ (20 μM heterodimer), UreB (20 μM monomer), or (UreABC)$_3$ (10 μM heterotrimer) in the same buffer. The mixtures were incubated at 42 °C for 1 h (previously shown to be optimal for binding of UreEF to MBP-UreD[10]), and aliquots were analyzed by SDS−PAGE. Amylose resin was equilibrated in TEB buffer containing 25 mM NaCl and added to each sample (at $^1/_4$ of the solution volume), and the slurries were gently rocked for 1 h at ambient temperature and centrifuged at 1000g. The supernatant solutions were discarded; the resins were washed five times with TEB buffer containing 25 mM NaCl (at volumes equivalent to that of the starting mixture, with the fifth wash reserved for SDS−PAGE analysis), and TEB buffer containing 25 mM NaCl and 10 mM maltose was added (again at a volume equivalent to that of the starting mixture). The slurries were vortexed and centrifuged at 4000g, and the supernatant solutions containing the eluted proteins were examined by SDS−PAGE. Prior studies with MBP alone had revealed no interaction with any urease-related protein.[10]

Amylose pull-down studies using MBP-UreD were conducted in a similar manner as described above, except that (UreABC)$_3$, (UreAC)$_3$, and UreB (initially in HT buffer) were diluted to their working concentrations in TEB with 25 mM NaCl. Equilibrated amylose resin was added to the incubations (total volumes of 500 μL) at $^1/_5$ of the mixture volumes.

Protease Stability Studies. Stock solutions of (UreAC)$_3$ and (UreABC)$_3$ in HT buffer were diluted to 2 μg/μL in TBS. Mixtures (10 μL) consisted of 1 μL (2 μg) of either (UreAC)$_3$ or (UreABC)$_3$, 1 μL of 0.1 μg/μL trypsin [sequencing grade, modified porcine trypsin, Promega; used at 1:20 ratio (w/w) of trypsin to protein sample], and 8 μL of TBS. These mixtures were incubated for 10, 30, or 60 min at 37 °C, and the reactions were stopped by the addition of SDS−PAGE loading buffer and boiling for 3 min. Control reaction mixtures lacking trypsin were incubated at 37 °C for 60 min in parallel. The digested samples were analyzed by SDS−PAGE.

■ RESULTS

Purification and Properties of UreB, UreBΔ1−19, and (UreAC)$_3$. To evaluate the function of UreB and its 19 N-terminal residues (a potential tether and hinge region) during urease activation, the full-length and truncated proteins were purified free of the partner subunits, UreA and UreC. Wild-type *ureB* and a *ureB* fragment lacking the nucleotides encoding residues 1−19 were cloned into pET-42b, resulting in pUreB and pUreBΔ1−19, respectively. These plasmids were transformed into *E. coli* BL21-Gold(DE3) cells for protein overproduction, and UreB and UreBΔ1−19 were isolated from cell-free extracts by successive chromatography on anion-exchange and gel filtration matrices (Figure 2C, lanes 2 and 3, respectively). The native molecular mass of purified UreB was estimated by Shodex KW-804 gel filtration chromatography in comparison to the retention time of a set of molecular mass standards, yielding a mass of 9490 ± 60 Da [average of triplicate determinations ± the standard deviation (SD)]. This result indicates that UreB (calculated molecular mass of 11.7 kDa) is a monomer in solution.

To purify (UreAC)$_3$ free of UreB, *ureA* and *ureC* were cloned into pETDuet-1, an expression vector containing two T7 RNA polymerase-driven transcription units (composed of independent T7 promoters, *lac* operators, ribosomal binding sites, and multiple-cloning sites) for the simultaneous production of two

proteins in the cell. The resultant vector, pUreAC, was transformed into *E. coli* BL21-Gold(DE3) for protein production, and (UreAC)$_3$ was isolated from cell-free extracts by successive chromatography on anion-exchange and hydrophobic-interaction matrices (Figure 2C, lane 1). The native molecular mass of purified (UreAC)$_3$ was estimated to be 171100 ± 680 Da (average of triplicate determinations ± SD) by using a Shodex KW-804 gel filtration column, equivalent to 2.4 UreAC heterodimers in the quaternary structure. A similar analysis using Superdex-200 resin yielded a molecular mass of 219000 Da, or 3.1 UreAC heterodimers per complex. Taken together, these data suggest that (UreAC)$_3$ exists as a trimer of heterodimers in solution.

The purified UreB, UreBΔ1−19, and (UreAC)$_3$ proteins were examined by CD spectroscopy to assess their secondary structures. Spectra for the full-length and truncated UreB proteins were similar (Figure 3A) and had the characteristic shape associated with a protein predominantly composed of β-sheets and random coils,[36] as expected from the crystal structure of this subunit within intact urease (3% α-helix, 38% β-sheet, and 59% random coil).[21] Attempts to predict the secondary structural elements of UreB by deconvolution programs were unsuccessful because of the low level of α-helix that is known to limit prediction analysis.[37] By contrast, the CD spectrum of (UreAC)$_3$ (Figure 3B) was readily deconvoluted by the K2D program of the Dichroweb server,[38] revealing a composition of 32% α-helix, 13% β-sheet, and 55% random coil. The proportions of these elements agree well with those in the corresponding components of the urease crystal structure (34% α-helix, 23% β-sheet, and 43% random coil).[21]

Formation of a Complex between (UreAC)$_3$ and UreB in Vitro. The ability of (UreAC)$_3$ to form a complex with UreB or UreBΔ1−19 in vitro was monitored by gel filtration chromatography (panel A or B of Figure 2, respectively). The mixtures of (UreAC)$_3$ with excess UreB or UreBΔ1−19 chromatographed as three distinct peaks of 280 nm-absorbing species. The first peak to elute from the mixture with UreB (peak 1) was a high-molecular mass species containing UreA, UreB, and UreC (Figure 2C, lane 4), demonstrating that UreB had formed a complex with (UreAC)$_3$. The (UreABC*)$_3$ sample [i.e., the complex of (UreAC)$_3$ and UreB] was examined by CD spectroscopy (Figure 3B), and its spectrum was similar to that of (UreAC)$_3$, suggesting that the small UreB subunit had little influence on the overall α-helical content. Peaks 2 and 3 of the same mixture both contained excess UreB that had not bound to (UreAC)$_3$ (Figure 2C, lanes 5 and 6); however, peak 3 also contained some low-molecular mass contamination likely arising from the UreB preparation. Comparison of the retention time of UreB in peak 2 with those of a set of molecular mass standards yielded a mass of 9600 Da, consistent with the monomeric form of the protein. The delayed elution position of UreB in peak 3 indicates this sample had interacted with the gel filtration matrix, thereby causing the appearance of two peaks containing UreB. Peak 1 of the (UreAC)$_3$/UreBΔ1−19 mixture appeared to contain only (UreAC)$_3$ (Figure 2C, lane 7); however, UreBΔ1−19 overlaps with UreA during SDS−PAGE. Gel scanning and integration of the bands for (UreAC)$_3$ yielded an apparent UreA:UreC ratio of 0.5:1, while peak 1 of the (UreAC)$_3$/UreBΔ1−19 sample yielded an apparent low-molecular mass species:UreC ratio of 0.4:1. If UreBΔ1−19 had formed a complex with (UreAC)$_3$, the resultant ratio of protein bands would have increased compared to that for (UreAC)$_3$; therefore, UreBΔ1−19 does not form a
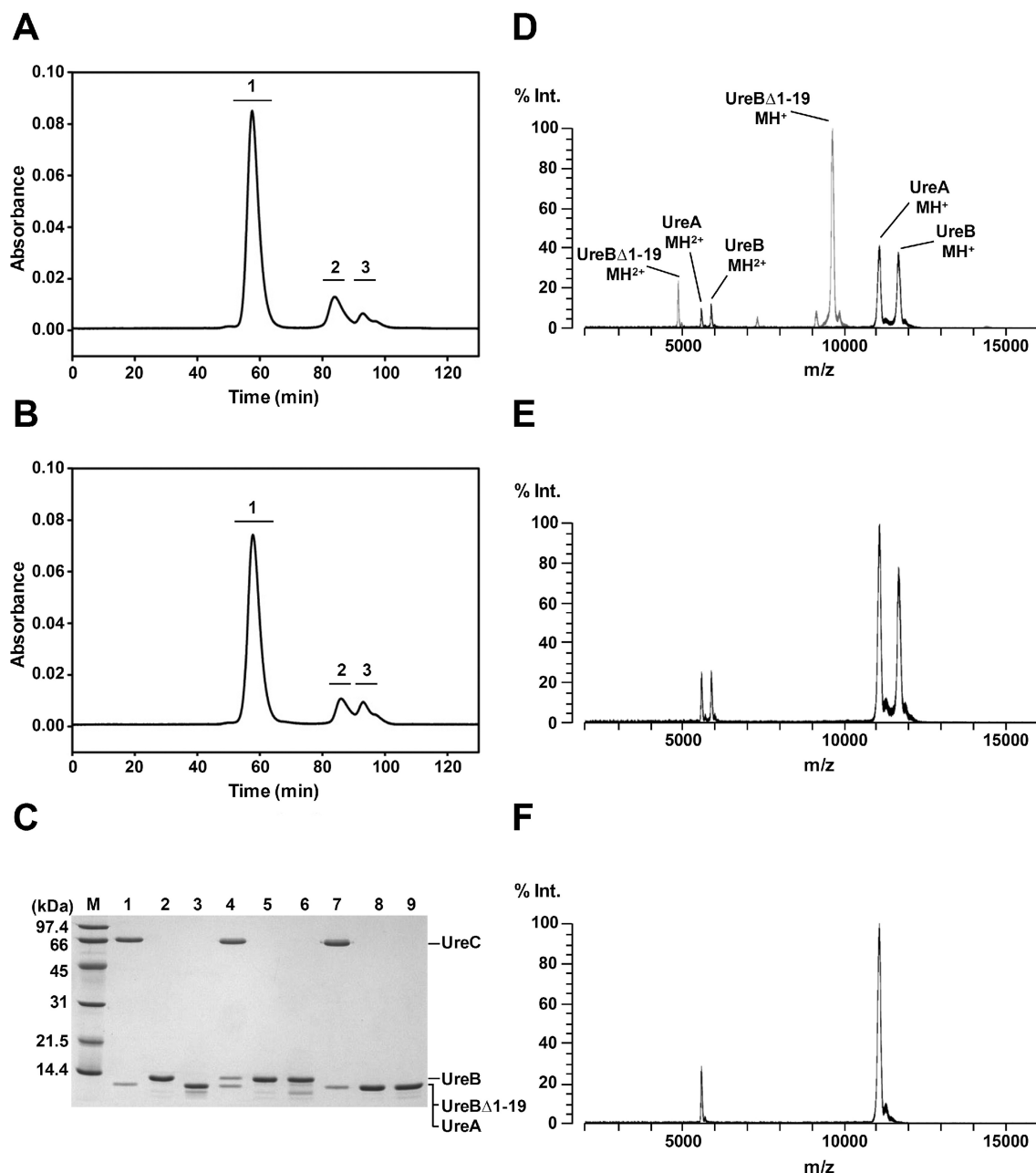
Figure 2. In vitro formation of a complex between $(UreAC)_3$ and UreB or $UreB\Delta1-19$. (A and B) Superdex-200 chromatogram of a mixture containing (A) $(UreAC)_3$ and excess UreB or (B) $(UreAC)_3$ and excess $UreB\Delta1-19$. (C) SDS−PAGE analysis of pure proteins (2 μg) and individual peaks (denoted by horizontal black bars and numbering, 2 μg) from panels A and B: lane M, molecular mass markers; lane 1, $(UreAC)_3$; lane 2, UreB; lane 3, $UreB\Delta1-19$; lane 4, $(UreAC)_3$ and UreB, peak 1; lane 5, same, peak 2; lane 6, same, peak 3; lane 7, $(UreAC)_3$ and $UreB\Delta1-19$, peak 1; lane 8, same, peak 2; lane 9, same, peak 3. (D−F) MALDI-TOF MS spectra (depicting the m/z range of 2000−16000) of (D) authentic $(UreABC)_3$ (black) overlaid with $UreB\Delta1-19$ (gray), (E) peak 1 of panel A, and (F) peak 1 of panel B.

complex with $(UreAC)_3$. For comparison, analysis of the protein bands derived from peak 1 of the $(UreAC)_3$/UreB sample provided an apparent UreA:UreB:UreC ratio of 0.5:0.5:1, similar to that found when native urease was subjected to this analysis, i.e., a UreA:UreB:UreC ratio of 0.7:0.6:1 (Figure 7, lane 1).

MALDI-TOF MS was used to further examine whether UreB and $UreB\Delta1-19$ bound to $(UreAC)_3$. As illustrated in Figure 2D, both small subunits were detected in authentic $(UreABC)_3$ with m/z values of 11119 and 11718 for the singly protonated species of UreA and UreB, respectively, and m/z values of 5610 and 5916 for the doubly protonated species, respectively. UreC also was detected near 60 kDa for this

sample, but its intensity was greatly diminished in comparison to those of the small subunits. Also shown in this panel are species associated with singly and doubly protonated $UreB\Delta1-19$, possessing m/z values of 9676 and 4894, respectively. Similar analysis of peak 1 from panel A provided the spectrum of panel E, demonstrating the presence of both UreA and UreB. By contrast, analysis of peak 1 of panel B revealed the clear presence of UreA and the absence of $UreB\Delta1-19$.

In Vitro Activation. When activated under standard conditions with varying Ni^{2+} concentrations, $(UreABC)_3$ and $(UreABC^*)_3$ both exhibited sigmoid-like activation profiles (Figure 4) with respect to an increasing Ni^{2+} concentration. $(UreABC)_3$ yielded a

A

B
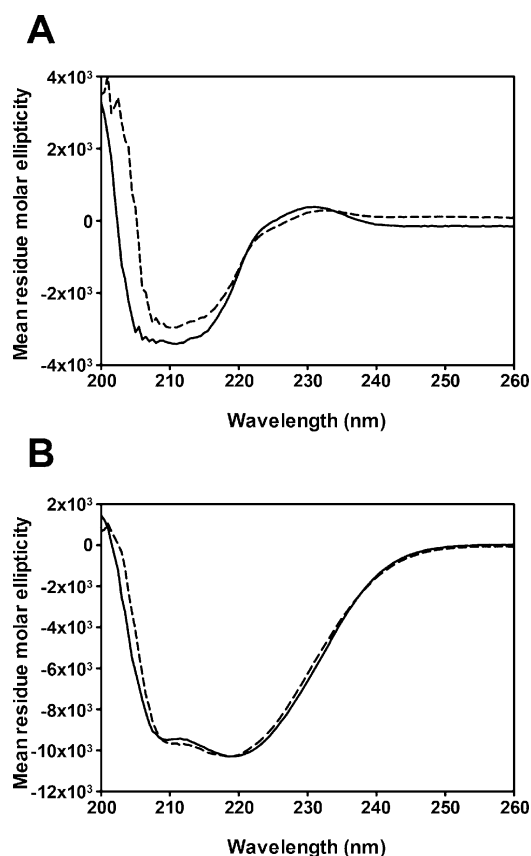
Figure 3. Secondary structure analysis of UreB, UreBΔ1−19, (UreAC)$_3$, and (UreABC*)$_3$. (A) Raw averaged CD spectra for UreB (---) and UreBΔ1−19 (—). (B) Raw averaged CD spectra for (UreAC)$_3$ (—) and (UreABC*)$_3$ (---).
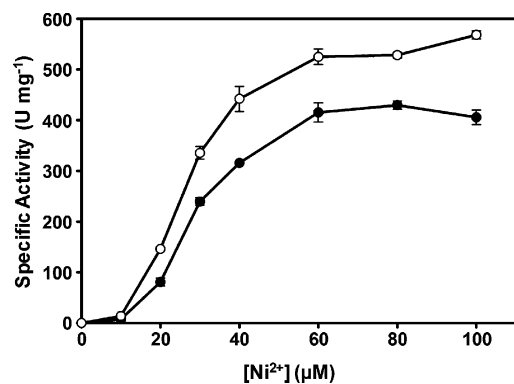
Figure 4. In vitro activation of (UreABC)$_3$ and (UreABC*)$_3$ as a function of varying Ni^{2+} concentrations. (UreABC)$_3$ (●) and (UreABC*)$_3$ (○) were incubated for 1 h in standard activation buffer containing the indicated concentrations of NiCl$_2$, and aliquots were assayed for urease activity. Data points represent the average of triplicate experiments ± SD.

specific activity of ∼400 units/mg of protein, as previously reported,[16,19,39] while (UreABC*)$_3$ generated even more activity, reaching ∼570 units/mg of protein (Figure 4 and Table 2). These results indicate that (UreABC*)$_3$ represents a functional form of the urease apoprotein with greater activation competence compared to the preformed apoprotein as isolated from the cells. By contrast, efforts to activate (UreAC)$_3$ under standard conditions led to negligible levels of activity (<0.2 unit/mg of

protein). Treatment of (UreAC)$_3$ under activation conditions followed by the addition of UreB led to a specific activity of 34.0 ± 1.9 units/mg of protein (average of triplicate experiments ± SD), consistent with the inability of UreB to trap and activate a preloaded UreC active site. By contrast, a mixture of (UreAC)$_3$ and excess UreBΔ1−19 subjected to activation conditions generated a specific activity of only 2.5 ± 0.1 units/mg of protein (average of triplicate experiments ± SD).

Metal Analyses of in Vitro Activated Species. To examine the effect of inclusion of UreB on Ni^{2+} incorporation into urease apoprotein, samples that had been subjected to the standard activation conditions were analyzed for metal content by ICP-AES (Table 2). For comparison, 0.53 equiv of Ni per heterotrimer was associated with authentic (UreABC)$_3$ apoprotein that was activated by use of standard conditions and treated with EDTA,[39] whereas 1.74 or 1.83 equiv of Ni was incorporated into the sample that was not treated with chelator.[19,39] When using (UreABC*)$_3$, obtained by mixing UreB with (UreAC)$_3$ before activation, the metal content of the EDTA-treated sample was 1.00 Ni per heterodimer, whereas samples not treated with chelator possessed 2.56 equiv of metal. In contrast, (UreAC)$_3$ subjected to activation conditions bound only 0.10 equiv of nickel if treated with chelator but still bound 2.57 equiv in the absence of EDTA. Finally, (UreAC)$_3$ that was activated and then mixed with UreB contained 0.18 equiv of nickel with EDTA treatment and 2.78 equiv of metal without the chelator.

In Vivo Interactions of MBP-UreD with (UreABC)$_3$, UreB, UreBΔ1−19, and (UreAC)$_3$. We investigated the in vivo interactions between a soluble form of UreD (i.e., the MBP-UreD fusion protein[10]) and (UreABC)$_3$, UreB, UreBΔ1−19, and (UreAC)$_3$ by using amylose resin affinity purification (i.e., amylose pull-down studies). *E. coli* BL21-Gold(DE3) cells were transformed with pCDF-MBP-UreD, a vector producing MBP-UreD, and either pEC004 [encoding (UreABC)$_3$[10]], pUreB, pUreBΔ1−19, or pUreAC. Soluble cell-free extracts from cultures induced with IPTG were subjected to amylose resin chromatography, and the samples were analyzed by SDS−PAGE and Western blotting using anti-*K. aerogenes* urease antibodies (Figure 5). Pull-down analysis of soluble extracts from cells cotransformed with pCDF-MBP-UreD and pEC004 revealed the copurification of (UreABC)$_3$ with MBP-UreD (Figure 5A, lane 2). This result was substantiated by the presence of urease cross-reactive bands in the cognate Western blot (Figure 5B, lane 2). A similar analysis of extracts from cells cotransformed with pCDF-MBP-UreD and pUreB revealed that UreB is copurified with MBP-UreD (Figure 5A,B, lane 4). In contrast, UreBΔ1−19 did not interact with MBP-UreD (Figure 5C, lane 2) when these proteins were coproduced in the cell. Finally, pull-down analysis of soluble extracts from cells cotransformed with pCDF-MBP-UreD and pUreAC indicates that (UreAC)$_3$ is copurified with MBP-UreD (Figure 5A,B, lane 6). In the latter sample, numerous cross-reactive protein bands were visible in the Western blot of the cell extracts and the amylose resin elution pool, consistent with partial degradation of UreC.

In Vitro Interactions of MBP-UreD and the MBP-UreD−UreF−UreG Complex with (UreABC)$_3$, UreB, and (UreAC)$_3$. The in vivo interaction results described above were extended by monitoring the in vitro formation of complexes between purified proteins. MBP-UreD and the soluble MBP-UreD−UreF−UreG heterotrimer were each mixed with (UreABC)$_3$, UreB, or (UreAC)$_3$ and monitored for complex

Table 2. Properties of Urease Apoprotein Samples Subjected to Activation Conditions[a]

apoprotein sample[b]	specific activity (units/mg of protein)	nickel content[c]
(UreABC*)$_3$	568 ± 8	1.00 ± 0.04 (2.56 ± 0.27)
(UreAC)$_3$	<0.2	0.10 ± 0.03 (2.57 ± 0.36)
(UreAC)$_3$, then add UreB	34.0 ± 1.9	0.18 ± 0.04 (2.78 ± 0.17)
(UreAC)$_3$ and UreBΔ1−19	2.5 ± 0.1	—[d]

[a]Standard activation conditions involved incubation of the apoprotein sample (5−10 μM) for 1 h at 37 °C in 100 mM HEPES (pH 8.3) containing 100 mM NaHCO$_3$, 150 mM NaCl, and 100 μM NiCl$_2$. [b](UreABC*)$_3$ is the complex derived from mixing (UreAC)$_3$ with UreB prior to incubation in activation buffer. (UreAC)$_3$ was subjected to activation conditions followed by incubation with UreB, or a mixture of (UreAC)$_3$ and excess UreBΔ1−19 was subjected to activation conditions. [c]The metal content is indicated per UreC protomer and was determined after removal of adventitious metal by treatment of the sample for 5 min with 10 mM EDTA followed by gel filtration chromatography. Numbers in parentheses are for samples not treated with EDTA but subjected to gel filtration chromatography. Specific activity and metal content values represent the average of triplicate experiments ± SD. [d]Metal content not determined.

formation by amylose resin chromatography followed by SDS−PAGE analysis. Despite its ability to interact with (UreABC)$_3$, UreB, and (UreAC)$_3$ in vivo (see above), MBP-UreD did not bind to these purified proteins in vitro (data not shown). In the same way, neither (UreAC)$_3$ (Figure 6, lane 4) nor UreB (lane 3) was copurified with the MBP-UreD−UreF−UreG complex (lane 1) as shown by the absence of the small subunit bands [and by the unchanged ratio of the MBP-UreD versus UreG and UreF band intensities, negating the presence of UreC for the (UreAC)$_3$ sample] in the eluted fractions (Figure 6, lanes 10 and 13). Conversely, (UreABC)$_3$ did bind to the MBP-UreD−UreF−UreG complex, which is made evident by the appearance of UreA and UreB bands (and by the increased relative intensity of the upper band compared to the UreG and UreF bands) in the elution fraction (Figure 6, lane 7). This result suggests that intact urease is required to interact in vitro with the preformed complex of the UreD, UreF, and UreG accessory proteins.

Protease Susceptibility Studies. To follow up on the observation that (UreAC)$_3$-derived UreC was degraded in soluble extracts from cells producing (UreAC)$_3$ and MBP-UreD, as revealed during the amylose resin pull-down studies (Figure 5A,B, lane 6), we monitored the protease susceptibility of selected samples. As a representative protease, trypsin was incubated with purified (UreAC)$_3$ and (UreABC)$_3$ at 37 °C, and aliquots were examined by SDS−PAGE over time (Figure 7). Several UreC digestion fragments were observed within 10 min of subjecting (UreABC)$_3$ to proteolysis, with little further change noted over the next 50 min. Conversely, UreC in (UreAC)$_3$ was completely digested within 10 min, and fewer fragments were visible at each subsequent time point, indicating an enhanced susceptibility of (UreAC)$_3$ in comparison with that of (UreABC)$_3$. The most prominent digestion fragment in the latter sample, which was also present in (UreABC)$_3$, has a molecular mass of ∼30 kDa.

DISCUSSION

A wealth of literature details the urease catalytic mechanism and activation process, primarily related to the dinuclear nickel metallocenter in the large subunits of the enzyme. By contrast, there is scant information available related to the roles of the protein's small subunits found in most bacterial enzymes or the corresponding domains of the fused subunits in *Helicobacter* species, fungi, and plants. In this work, we have focused on the role of UreB in urease activation through several lines of investigation.

As a first step in our analysis, we engineered cells to separately produce UreB, UreBΔ1−19 (a truncated form of UreB missing a putative hinge and tether region), and (UreAC)$_3$. Our subsequent

purifications represent the first examples of isolated UreB subunits and UreB-free urease. UreB was demonstrated to be a soluble monomer composed solely of β-sheets and random coils according to gel filtration chromatography and CD spectroscopy. UreBΔ1−19 was purified in the same manner and shared a similar size and CD spectrum. By contrast, (UreAC)$_3$ was established as a trimer of the heterodimer and shown to contain substantial amounts of α-helix (32%). The secondary structure estimations provided by CD spectroscopy are in good agreement with the appropriate components of the crystal structure of *K. aerogenes* urease[21] (note the α-helix-free structure of UreB and the α-helix-rich structure of UreA and UreC in Figure 1); thus, UreB, UreBΔ1−19, and (UreAC)$_3$ appear to adopt structures similar to that in the native protein, confirming their utility for functionality studies.

We next examined whether UreB or UreBΔ1−19 could bind spontaneously to (UreAC)$_3$ and thus generate a functional urease apoprotein. Incubation of UreB and (UreAC)$_3$ for only 15 min yielded the stable (UreABC*)$_3$ species. The apparent noninteger UreA:UreB:UreC ratio (∼0.5:∼0.5:1) found during SDS−PAGE analysis of this species and authentic urease apoprotein is attributed to differential binding of the anionic dye to the variably charged subunits. The MALDI-TOF MS results clearly demonstrate that UreBΔ1−19 does not spontaneously bind to (UreAC)$_3$. These results are attributed to the absence of residues 2−8 from the N-terminus of UreB that are known to form the terminal strand of a β-sheet that is primarily composed of β-strands from UreC,[29] thus underscoring the importance of this tether region for UreB−UreC interaction. The main domain of UreB exhibits few polar and hydrophobic interactions with UreC, accounting for the inability of the truncated protein to bind to UreC.

The in vitro activation competence of (UreABC)$_3$ and that of its reconstituted version were compared to validate the functionality of (UreABC*)$_3$. Both species exhibited a sigmoid-like activation behavior with respect to varied Ni^{2+} concentrations, a previously unreported observation. We attribute the sigmoidicity to the need for incorporating two atoms of nickel per active site, a process that is promoted by greater metal ion concentrations. (UreABC)$_3$ was maximally activated to ∼400 units/mg of protein, as was previously observed,[16] equating to 16% of the nascent active sites gaining activity. Unexpectedly, (UreABC*)$_3$ was activated to even greater levels, reaching a maximal specific activity of ∼570 units/mg of protein (Figure 4). On the basis of single ICP-AES analyses of purified (UreABC)$_3$ (yielding 0.3 iron and 0.1 zinc) and (UreAC)$_3$, (providing undetectable levels of any metal), we hypothesize that the decreased activation competence of the apoprotein purified from the cell compared to that formed by mixing UreB
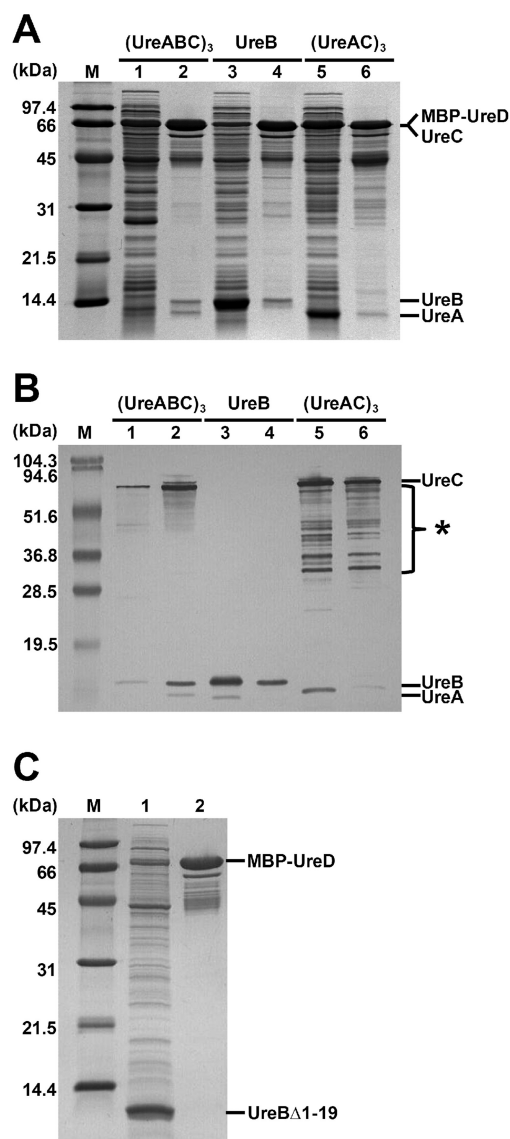
Figure 5. In vivo interactions of MBP-UreD with $(UreABC)_3$, UreB, $(UreAC)_3$, and UreBΔ1−19. (A) SDS−PAGE gel depicting the interactions of MBP-UreD with $(UreABC)_3$, UreB, and $(UreAC)_3$. *E. coli* BL21-Gold(DE3) cells were cotransformed with pCDF-MBP-UreD (encoding MBP-UreD) and either pEC004, pUreB, or pUreAC [encoding $(UreABC)_3$, UreB, or $(UreAC)_3$, respectively]. Soluble cell-free extracts of IPTG-induced cultures (10 μg, odd-numbered lanes) and proteins eluted from amylose resin upon addition of maltose (5 μg, even-numbered lanes) were subjected to SDS−PAGE and stained with Coomassie brilliant blue. (B) Western blot of the same samples. Each sample (1 μg) was subjected to SDS−PAGE, electroblotted onto an Immobilon membrane, and blotted with anti-*K. aerogenes* urease antibodies. The asterisk indicates the migration positions of cross-reactive bands that may represent UreC degradation products. (C) Interaction of MBP-UreD with UreBΔ1−19. Studies analogous to those whose results are shown in panel A were conducted, but using cells that produce MBP-UreD and UreBΔ1−19. In each panel, M indicates molecular mass markers.

with $(UreAC)_3$ relates to non-nickel metal contamination of $(UreABC)_3$ compared to metal-free $(UreAC)_3$. Regardless of the explanation, these results confirm the efficacy of $(UreABC*)_3$ as a functional urease apoprotein.

To gain insight into the role of UreB during in vitro activation, $(UreAC)_3$ was subjected to the standard activation conditions, and negligible levels of activity were detected. All residues that coordinate the metallocenter or participate in catalysis are present in the UreB-free protein, yet a functional active site was not produced. It was conceivable that the activation conditions did lead to normal metalation of the protein, but the lack of UreB caused a conformational change in $(UreAC)_3$ that hindered substrate access, restricted movement of a flap containing a catalytic residue that covers the active site, or otherwise stifled activity. To test this possibility, UreB was added to a preparation of $(UreAC)_3$ that had been incubated under standard activation conditions. A small fraction of active enzyme was generated [i.e., yielding a specific activity of 34 units/mg of protein, or 6% of that for maximally activated $(UreABC*)_3$], but this likely arises from UreB associating with low levels of the $(UreAC)_3$ apoprotein followed by partial activation. For comparison, a mixture of $(UreAC)_3$ and excess UreBΔ1−19 that had been treated under activation conditions yielded less than $^1/_{10}$ of the activity found when using UreB. In sum, full-length UreB must bind to $(UreAC)_3$ prior to exposure to Ni^{2+} and bicarbonate to exert its positive effect on the activation process.

In addition to measurement of the urease activities of various samples following in vitro activation, it was of interest to quantify their nickel contents. After $(UreABC)_3$ had been subjected to activation conditions, nearly two nickels per hetero-trimer were present.[19,39] When this sample was subsequently incubated with EDTA, the metal content was reduced to 0.53 equiv,[39] but activity was unaffected. Activation of $(UreABC*)_3$ leads to 2.56 equiv of bound nickel, but this is reduced to 1.00 equiv in the presence of EDTA. The increased level of tightly bound Ni^{2+} correlates well with the greater activity of this sample versus that for activated $(UreABC)_3$. Significantly, when $(UreAC)_3$ is subjected to the same activation conditions (but yielding negligible levels of activity), it contains 2.57 equiv of nickel without chelator that is reduced to only 0.10 equiv when treated with EDTA, suggesting that UreB protects the metallocenter from chelation. When $(UreAC)_3$ is first subjected to activation conditions, incubated with UreB, and finally treated with EDTA, a low level of additional metal is bound compared to that with $(UreAC)_3$ alone. This result demonstrates that UreB cannot trap a preformed metallo-center; instead, this subunit must be present to generate the properly bound metal complex.

The interaction of *K. aerogenes* UreD with urease was previously examined by using amylose resin pull-down studies with the MBP-UreD fusion protein[10] along with chemical cross-linking and small-angle X-ray scattering analyses of the $(UreABC)_3$−UreD protein complex.[28,29] Interactions among these proteins from other organisms also were investigated by using yeast two-hybrid and immunoprecipitation methods.[40−42] These efforts provided evidence that UreD interacts with both UreB and UreC, consistent with UreD binding to the vertices of the urease triangular structure. To obtain further details about these UreD interactions, we extended the amylose resin pull-down approach, both in vivo and in vitro, to study binding of MBP-UreD to UreB, UreBΔ1−19, $(UreAC)_3$, and control $(UreABC)_3$. Pull-down analyses of extracts from cells producing MBP-UreD along with UreB, $(UreAC)_3$, or $(UreABC)_3$ all demonstrated binding between the paired components, whereas cellular MBP-UreD and UreBΔ1−19 did not form a complex. These results suggest binding can occur between UreD and UreC, confirm a direct interaction between UreD and UreB, and underscore the importance of the
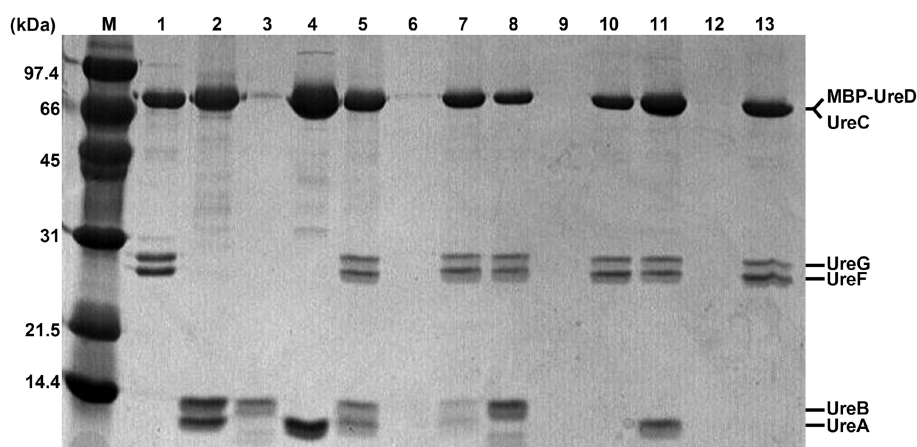
Figure 6. In vitro interactions of the MBP-UreD−UreF−UreG complex with $(UreABC)_3$, $(UreAC)_3$, and UreB. The MBP-UreD−UreF−UreG complex (2 μM) was mixed with $(UreABC)_3$ (10 μM heterotrimer), $(UreAC)_3$ (20 μM heterodimer), or UreB (20 μM), incubated at 42 °C, and chromatographed on amylose resin, and bound protein complexes were eluted in a buffer containing maltose. Samples analyzed by SDS−PAGE included the mixtures prior to chromatography, the final washes before elution, and the eluted complexes: lane M, molecular mass markers; lane 1, MBP-UreD−UreF−UreG complex; lane 2, $(UreABC)_3$; lane 3, UreB; lane 4, $(UreAC)_3$; lane 5, MBP-UreD−UreF−UreG complex and $(UreABC)_3$ prior to chromatography; lane 6, final wash prior to elution; lane 7, elution; lane 8, MBP-UreD−UreF−UreG complex and UreB prior to chromatography; lane 9, final wash prior to elution; lane 10, elution; lane 11, MBP-UreD−UreF−UreG complex and $(UreAC)_3$ prior to chromatography; lane 12, final wash prior to elution; lane 13, elution.
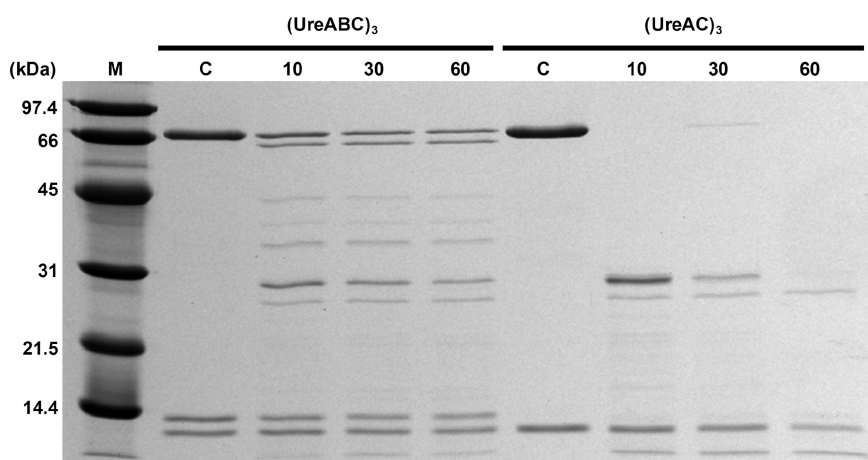
Figure 7. Trypsin proteolysis of $(UreABC)_3$ and $(UreAC)_3$. Two micrograms of either $(UreABC)_3$ or $(UreAC)_3$ was incubated with 0.1 μg of trypsin at 37 °C for 10, 30, or 60 min as indicated above each lane, and samples were analyzed by SDS−PAGE. Nondigested control samples are indicated by C, and molecular mass markers are denoted by M.

N-terminal region of UreB for the latter interaction. Because the CD spectrum of UreBΔ1−19 is essentially identical to that of UreB and consistent with the fold of UreB in the crystal structure, the lack of interaction between UreBΔ1−19 and MBP-UreD specifically relates to the missing N-terminus, not to a misfolded protein. When the interactions of MBP-UreD with the other proteins were examined in vitro, the results were quite different. Purified MBP-UreD and $(UreABC)_3$ proteins do not form a complex, as previously described,[10] nor does MBP-UreD bind UreB or $(UreAC)_3$. We attribute these results to a requirement for an unidentified cellular constituent (i.e., a protein chaperone or small molecule) that facilitates the interaction between these components. Alternatively, it is possible that purified MBP-UreD is structurally different from the form (perhaps partially unfolded) that interacts with UreB, $(UreAC)_3$, and $(UreABC)_3$ in vivo.

We also examined the in vitro interactions of UreD with the urease subunits by making use of the MBP-UreD−UreF−UreG complex.[10] Amylose pull-down studies with the heterotrimeric

complex of accessory proteins demonstrated binding to $(UreABC)_3$, but not to $(UreAC)_3$ or UreB. This result suggests that the added presence of UreF and UreG in the complex containing MBP-UreD modifies its properties such as to allow binding to fully assembled urease. This result is similar to what was observed in vivo using cells that produce MBP-UreD and $(UreABC)_3$, hinting that a cellular protein mimicking UreF and/or UreG is involved in that interaction. In contrast, binding of the MBP-UreD−UreF−UreG complex to the urease apoprotein missing UreB or to the isolated UreB subunit is precluded, suggesting a greater specificity in this interaction than for the in vivo binding with MBP-UreD.

The anti-*K. aerogenes* urease Western blot analyzed as part of the in vivo interaction studies revealed numerous cross-reactive bands in extracts of cells producing $(UreAC)_3$, whereas the other samples were free of these contaminants. These bands are likely to be UreC degradation products, consistent with enhanced proteolysis of $(UreAC)_3$ compared to $(UreABC)_3$. Follow-up studies provided clear evidence that $(UreAC)_3$ is

proteolyzed by trypsin at a faster rate than (UreABC)$_3$, suggesting that, in addition to its role in urease activation, UreB protects the apoprotein from spurious proteolysis in vivo. Analysis of the *K. aerogenes* urease crystal structure[21] indicates that Arg339 of UreC is moderately exposed in the wild-type protein, but the absence of UreB may lead to increased protease susceptibility involving this residue. Similarly, the loss of UreB could reasonably expose Arg52 to the protease.

In conclusion, our results demonstrate that UreB stimulates the productive binding of nickel to the urease apoprotein and stabilizes it against chelation. Moreover, UreB acts as an important interface between the active site-containing UreC subunit and the accessory proteins, with residues 1−19 being critical for this interaction. Finally, UreB protects the urease apoprotein from proteolysis. This work, the first study focused on the function of UreB, establishes the central importance of this subunit to the enzyme. The important roles of UreB in *K. aerogenes* are likely to be replicated in other three-subunit bacterial ureases and by the corresponding domains in the *Helicobacter*, fungal, and plant enzymes.

■ AUTHOR INFORMATION

Corresponding Author

*Address: 2215 Biomedical Physical Sciences, Michigan State University, East Lansing, MI 48824. Telephone: (517) 884-5404. Fax: (517) 353-8957. E-mail: hausinge@msu.edu.

■ ACKNOWLEDGMENTS

■ ABBREVIATIONS

β-ME, 2-mercaptoethanol; CD, circular dichroism; EDTA, ethylenediaminetetraacetic acid; HEPES, 4-(2-hydroxyethyl)-piperazine-1-ethanesulfonic acid; ICP-AES, inductively coupled plasma-atomic emission spectroscopy; IPTG, isopropyl β-D-1-thiogalactopyranoside; MBP, maltose binding protein; MWCO, molecular weight cutoff; PCR, polymerase chain reaction; TCEP, tris(2-carboxyethyl)phosphine hydrochloride; Tris, 2-amino-2-(hydroxymethyl)-1,3-propanediol; SDS−PAGE, sodium dodecyl sulfate−polyacrylamide gel electrophoresis.

■ REFERENCES

(1) Carter, E. L., Flugga, N., Boer, J. L., Mulrooney, S. B., and Hausinger, R. P. (2009) Interplay of metal ions and urease. *Metallomics* 1, 207−221.

(2) Zambelli, B., Musiani, F., Benini, S., and Ciurli, S. (2011) Chemistry of Ni^{2+} in urease: Sensing, trafficking, and catalysis. *Acc. Chem. Res. 44*, 520−530.

(3) Mobley, H. L. T., Island, M. D., and Hausinger, R. P. (1995) Molecular biology of microbial ureases. *Microbiol. Rev. 59*, 451−480.

(4) Witte, C.-P. (2011) Urea metabolism in plants. *Plant Sci. 180*, 431−438.

(5) Mobley, H. L. T., and Hausinger, R. P. (1989) Microbial ureases: Significance, regulation, and molecular characterization. *Microbiol. Rev. 53*, 85−108.

(6) Sumner, J. B. (1926) The isolation and crystallization of the enzyme urease. *J. Biol. Chem. 69*, 435−441.

(7) Dixon, N. E., Gazzola, C., Blakeley, R. L., and Zerner, B. (1975) Jack bean urease (EC 3.5.1.5). A metalloenzyme. A simple biological role for nickel? *J. Am. Chem. Soc. 97*, 4131−4133.

(8) Lee, M. H., Pankratz, H. S., Wang, S., Scott, R. A., Finnegan, M. G., Johnson, M. K., Ippolito, J. A., Christianson, D. W., and Hausinger, R. P. (1993) Purification and characterization of *Klebsiella aerogenes* UreE protein: A nickel-binding protein that functions in urease metallocenter assembly. *Protein Sci. 2*, 1042−1052.

(9) Park, I.-S., Carr, M. B., and Hausinger, R. P. (1994) *In vitro* activation of urease apoprotein and role of UreD as a chaperone required for nickel metallocenter assembly. *Proc. Natl. Acad. Sci. U.S.A. 91*, 3233−3237.

(10) Carter, E. L., and Hausinger, R. P. (2010) Characterization of *Klebsiella aerogenes* urease accessory protein UreD in fusion with the maltose binding protein. *J. Bacteriol. 192*, 2294−2304.

(11) Salomone-Stagni, M., Zambelli, B., Musiani, F., and Ciurli, S. (2007) A model-based proposal for the role of UreF as a GTPase-activating protein in the urease active site biosynthesis. *Proteins 68*, 749−761.

(12) Kim, J. K., and Hausinger, R. P. (2006) The UreEF fusion protein provides a soluble and functional form of the UreF urease accessory protein. *J. Bacteriol. 188*, 8413−8420.

(13) Lam, R., Romanov, V., Johns, K., Battaile, K., Wu-Brown, J., Guthrie, J. L., Hausinger, R. P., Pai, E., and Chirgadze, N. Y. (2010) Structure of a truncated urease accessory protein UreF from *Helicobacter pylori*. *Proteins 78*, 2839−2848.

(14) Boer, J. L., Quiroz-Valenzuela, S., Anderson, K. L., and Hausinger, R. P. (2010) Mutagenesis of *Klebsiella aerogenes* UreG to probe nickel binding and interactions with other urease-related proteins. *Biochemistry 49*, 5859−5869.

(15) Moncrief, M. B. C., and Hausinger, R. P. (1997) Characterization of UreG, identification of a UreD-UreF-UreG complex, and evidence suggesting that a nucleotide-binding site in UreG is required for in vivo metallocenter assembly of *Klebsiella aerogenes* urease. *J. Bacteriol. 179*, 4081−4086.

(16) Park, I.-S., and Hausinger, R. P. (1995) Requirement of carbon dioxide for in vitro assembly of the urease nickel metallocenter. *Science 267*, 1156−1158.

(17) Moncrief, M. B. C., and Hausinger, R. P. (1996) Purification and activation properties of UreD-UreF-urease apoprotein complexes. *J. Bacteriol. 178*, 5417−5421.

(18) Soriano, A., and Hausinger, R. P. (1999) GTP-dependent activation of urease apoprotein in complex with the UreD, UreF, and UreG accessory proteins. *Proc. Natl. Acad. Sci. U.S.A. 96*, 11140−11144.

(19) Park, I.-S., and Hausinger, R. P. (1996) Metal ion interactions with urease and UreD-urease apoproteins. *Biochemistry 35*, 5345−5352.

(20) Soriano, A., Colpas, G. J., and Hausinger, R. P. (2000) UreE stimulation of GTP-dependent urease activation in the UreD-UreF-UreG-urease apoprotein complex. *Biochemistry 39*, 12435−12440.

(21) Jabri, E., Carr, M. B., Hausinger, R. P., and Karplus, P. A. (1995) The crystal structure of urease from *Klebsiella aerogenes*. *Science 268*, 998−1004.

(22) Pearson, M. A., Michel, L. O., Hausinger, R. P., and Karplus, P. A. (1997) Structure of Cys319 variants and acetohydroxamate-inhibited *Klebsiella aerogenes* urease. *Biochemistry 36*, 8164−8172.

(23) Benini, S., Rypniewski, W. R., Wilson, K. S., Ciurli, S., and Mangani, S. (1998) The complex of *Bacillus pasteurii* urease with ß-mercaptoethanol from X-ray data at 1.65-Å resolution. *J. Biol. Inorg. Chem. 3*, 268−273.

(24) Benini, S., Rypniewski, W. R., Wilson, K. S., Miletti, S., Ciurli, S., and Mangani, S. (1999) A new proposal for urease mechanism based on the crystal structures of the native and inhibited enzyme from *Bacillus pasteurii*: Why urea hydrolysis costs two nickels. *Structure 7*, 205−216.

(25) Ha, N.-C., Oh, S.-T., Sung, J. Y., Cha, K.-A., Lee, M. H., and Oh, B.-H. (2001) Supramolecular assembly and acid resistance of *Helicobacter pylori* urease. *Nat. Struct. Biol. 8*, 505−509.

(26) Balasubramanian, A., and Ponnuraj, K. (2010) Crystal structure of the first plant urease from jack bean: 83 years of journey from its first crystal to molecular structure. *J. Mol. Biol. 400*, 274−283.

(27) Carter, E. L., Tronrud, D. E., Taber, S. R., Karplus, P. A., and Hausinger, R. P. (2011) Iron-containing urease in a pathogenic bacterium. *Proc. Natl. Acad. Sci. U.S.A. 108*, 13095−13099.

(28) Chang, Z., Kuchar, J., and Hausinger, R. P. (2004) Chemical crosslinking and mass spectrometric identification of sites of interaction for UreD, UreF, and urease. *J. Biol. Chem. 279*, 15305−15313.

(29) Quiroz-Valenzuela, S., Sukuru, S. C. K., Hausinger, R. P., Kuhn, L. A., and Heller, W. T. (2008) The structure of urease activation complexes examined by flexibility analysis, mutagenesis, and small-angle X-ray scattering. *Arch. Biochem. Biophys. 480*, 51−57.

(30) Sambrook, J., Fritsch, E. F., and Maniatis, T. (1989) *Molecular cloning: A laboratory manual*, 2nd ed., Cold Spring Harbor Laboratory Press, Plainview, NY.

(31) Colpas, G. J., Brayman, T. G., Ming, L.-J., and Hausinger, R. P. (1999) Identification of metal-binding residues in the *Klebsiella aerogenes* urease nickel metallochaperone, UreE. *Biochemistry 38*, 4078−4088.

(32) Weatherburn, M. W. (1967) Phenol-hypochlorite reaction for determination of ammonia. *Anal. Chem. 39*, 971−974.

(33) Laemmli, U. K. (1970) Cleavage of structural proteins during the assembly of the head of bacteriophage T4. *Nature 227*, 680−685.

(34) Quiroz-Valenzuela, S. (2008), New insights in the urease activation process obtained by characterization of apourease complexes and the UreG accessory protein of *Klebsiella aerogenes*. Ph.D. Thesis, Michigan State University, East Lansing, MI.

(35) Todd, M. J., and Hausinger, R. P. (1987) Purification and characterization of the nickel-containing multicomponent urease from *Klebsiella aerogenes*. *J. Biol. Chem. 262*, 5963−5967.

(36) Greenfield, N. J., and Fasman, G. D. (1969) Computed circular dichroism spectra for the evaluation of protein conformation. *Biochemistry 8*, 4108−4116.

(37) Whitmore, L., and Wallace, B. A. (2008) Protein secondary structure analyses from circular dichroism spectroscopy: Methods and reference databases. *Biopolymers 89*, 392−400.

(38) Whitmore, L., and Wallace, B. A. (2004) DICHROWEB, an online server for protein secondary structure analyses from circular dichroism spectroscopic data. *Nucleic Acids Res. 32*, W668−W673.

(39) Yamaguchi, K., Cosper, N. J., Stalhanske, C., Scott, R. A., Pearson, M. A., Karplus, P. A., and Hausinger, R. P. (1999) Characterization of metal-substituted *Klebsiella aerogenes* urease. *J. Biol. Inorg. Chem. 4*, 468−477.

(40) Rain, J.-C., Selig, L., de Reuse, H., Battaglia, V., Reverdy, C., Simon, S., Lenzen, G., Petel, F., Wojcik, J., Schächter, V., Chemama, Y., Labigne, A., and Legrain, P. (2001) The protein-protein interaction map of *Helicobacter pylori*. *Nature 409*, 211−215.

(41) Voland, P., Weeks, D. L., Marcus, E. A., Prinz, C., Sachs, G., and Scott, D. (2003) Interactions among the seven *Helicobacter pylori* proteins encoded by the urease gene cluster. *Liver Physiol. 284*, G96−G106.

(42) Heimer, S. R., and Mobley, H. L. (2001) Interaction of *Proteus mirabilis* urease apoprotein and accessory proteins identified with yeast two-hybrid technology. *J. Bacteriol. 183*, 1423−1433.

(43) Lee, M. H., Mulrooney, S. B., Renner, M. J., Markowicz, Y., and Hausinger, R. P. (1992) *Klebsiella aerogenes* urease gene cluster: Sequence of *ureD* and demonstration that four accessory genes (*ureD*, *ureE*, *ureF*, and *ureG*) are involved in nickel metallocenter biosynthesis. *J. Bacteriol. 174*, 4324−4330.